CHEMISTRY
A EUROPEAN JOURNAL

DOI: 10.1002/chem.201000640

Hole-Transfer Dyads and Triads Based on Perylene Monoimide, Quaterthiophene, and Extended Tetrathiafulvalene

Julien Boixel,[a] Errol Blart,[a] Yann Pellegrin,[a] Fabrice Odobel,*[a] Nicola Perin,[b] Claudio Chiorboli,[c] Sandro Fracasso,[b] Marcella Ravaglia,[b] and Franco Scandola*[b, d]

Abstract: Two families of dyad and triad systems based on perylene monoimide (PMI), quaterthiophene (QT), and 9,10-bis(1,3-dithiol-2-ylidene)-9,10-dihydroanthracene (extended tetrathiafulvalene, exTTF) molecular components have been designed and synthesized. The dyads (**D1** and **D2**) are of the PMI–QT type and the triads (**T1** and **T2**) of the PMI–QT–exTTF type. The two families differ in the saturated or unsaturated nature of the linker groups (ethynylene in **D1** and **T1**, ethylene in **D2** and **T2**) that bridge the molecular components. The dyads and triads have been characterized by electrochemical, photophysical, and computational methods. Both the experimental and the computational (DFT) results indicate that in the unsaturated systems strong intercomponent interactions lead to substantial perturbation of the properties of the subunits. In particular, in **T1**, delocalization is particularly effective between the QT and exTTF units, which would be better viewed combined as a single electronic subsystem. For the dyad systems, the photophysics observed following excitation of the PMI unit is solvent-dependent. In moderately polar solvents (dichloromethane, diethyl ether) fast charge separation is followed by recombination to the ground state. In toluene, slow conversion to the charge-separated state is followed by intersystem crossing and recombination to yield the triplet state of the PMI unit. The behavior of the triads, on the other hand, is remarkably similar to that of the corresponding dyads, which indicates that, after primary charge separation, hole shift from the oxidized QT component to exTTF is quite inefficient. This unexpected result has been rationalized on the basis of the anomalous (simultaneous two-electron oxidation) electrochemistry of exTTF and with the help of DFT calculations. In fact, although exTTF is electrochemically easier to oxidize than QT by around 0.6 V, the one-electron redox orbitals (HOMOs) of the two units in triad **T2** are almost degenerate.

Keywords: charge separation · donor–acceptor systems · electron transfer · photophysics · time-resolved spectroscopy

Introduction

The rational molecular design of photomolecular assemblies for efficient light-induced charge separation is a topic of considerable importance owing to its fundamental and practical implications for solar energy conversion (artificial photosynthesis[1–5] and photovoltaics[6–8]). Towards this goal, the general approach, which is essentially inspired by the strategy adopted by Nature in photosynthesis, involves creating a multistep electron-transfer chain along a molecular assembly that exhibits a defined redox gradient that allows the vectorial spatial separation of the photogenerated charges. In this context, many covalently linked donor–bridge–acceptor (D–B–A) systems have been prepared.[5,9–12] To produce a long-lived charge-separated state with high quantum yield, it is essential to maximize the rate of forward charge separation while reducing the rate of charge recombination by separating the two photogenerated charges over a large distance. So far the vast majority of triads designed for multistep elec-

[a] Dr. J. Boixel, Dr. E. Blart, Dr. Y. Pellegrin, Dr. F. Odobel
Chimie et Interdisciplinarité: Synthèse, Analyse, Modélisation (CEISAM)
Université de Nantes, CNRS UMR CNRS n° 6230
2, rue de la Houssinière
BP 92208–44322 Nantes Cedex 3 (France)
Fax: (+33) 251125402
E-mail: Fabrice.Odobel@univ-nantes.fr

[b] N. Perin, S. Fracasso, Dr. M. Ravaglia, Prof. F. Scandola
Dipartimento di Chimica, Universita' di Ferrara
via L. Borsari 46, 44100 Ferrara (Italy)
Fax: (+39) 0532240709
E-mail: snf@unife.it

[c] C. Chiorboli
ISOF-CNR, Sezione di Ferrara, via L. Borsari 46
44100 Ferrara (Italy)

[d] Prof. F. Scandola
Centro di Ricerca Interuniversitario per la Conversione Chimica dell'Energia Solare
Sezione di Ferrara, 44100 Ferrara (Italy)

Supporting information for this article is available on the WWW under http://dx.doi.org/10.1002/chem.201000640.

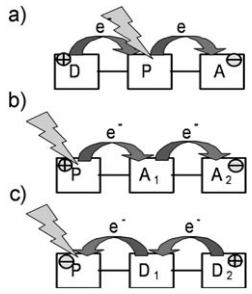

Figure 1. Schematic representation of the photoinduced charge separation in different types of triads.

tron transfer are of the type shown in Figure 1 a,b, that is, based on a light-absorbing unit (photosensitizer, P) sandwiched between a donor (D) and an acceptor (A) to form a triad of the type D–P–A or a photosensitizer covalently linked to several electron acceptors to give a triad of type $P–A_1–A_2$.[9–12] In the first case, the charge-separation process takes place by sequential electron- and hole-transfer processes,[5,11–16] whereas in the second, the charge separation takes place through two sequential electron-transfer steps.[17,18]

The reverse design, that is, the development of triads consisting of an electron-acceptor photosensitizer linked to different electron donors (such as $P–D_1–D_2$, Figure 1c) in which the photosensitizer decays by reductive quenching followed by a cascade hole transfer chain, are rare.[19–22] We have previously designed and reported bis-porphyrin-based photomolecular systems that undergo fast single-step photoinduced electron transfer over distances of 20–45 Å by a superexchange mechanism.[23–25] However, the very fast and efficient forward photoinduced charge separation was obtained at the expense of an also fast charge recombination, which precludes the formation of a long-lived charge-separated state. Herein, we describe two new molecular triads of the type $P–D_1–D_2$ (**T1** and **T2**; Scheme 1), designed to explore the possibility of extending the lifetime of the charge-separated state by a hopping mechanism. In this study the first electron donor is quaterthiophene (QT) because it is a rigid π-conjugated molecule, the electronic properties of which have been proved to be particularly suitable for acting as an effective bridging group or electron donor in molecular systems for photoinduced charge separation. For example, Otsubo and co-workers reported several interesting fullerene- or porphyrin-based photochemical systems connected to oligothiophenes, mostly oriented towards the development of plastic solar cells.[6,26–29] Perylene monoimide (PMI) is an attractive light collector to use for our purpose because it displays quite high molar absorptivity and strong electron-acceptor characteristics suitable in its photoexcited state for pulling away an electron from the quaterthiophene unit.[30] Furthermore, the radical anion of PMI exhibits a clear spectroscopic signature, which will ease the photophysical characterization.[31] In addition, PMI was previously connected to an oligothiophene chain and photoinduced charge separation was evidenced.[19,32–34] Finally, the 9,10-bis(1,3-dithiol-2-ylidene)-9,10-dihydroanthracene, also known as extended tetrathiafulvalene (exTTF), is an excellent electron donor, which has previously been used as a component in photomolecular arrays.[8,35–40] Another attractive feature of exTTF is its bis-electron-donating capability, which makes it a potentially useful molecule to serve as a hole reservoir for photoaccumulative electron transfer.[41–46]

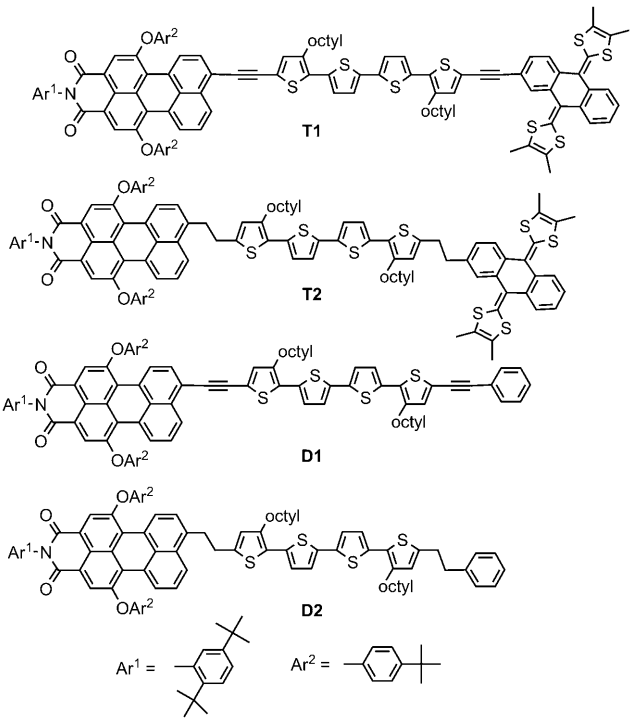

Scheme 1. Structures of the dyads and triads studied in this work.

We describe herein the synthesis and extensive characterization of original photomolecular triads and demonstrate that photoinduced hole transfer between PMI and quaterthiophene is a very fast process, irrespective of the solvent and the linkage between these units. Surprisingly, in spite of the presumably large driving force, the secondary hole-shift reaction ($^{-}P–D_1^{+}–D_2 \rightarrow {}^{-}P–D_1–D_2^{+}$) was not observed in these triads. Quantum chemical calculations have been used to rationalize this unexpected behavior, namely by showing that the first oxidation potential of exTTF is underestimated when determined by cyclic voltammetry.

Results and Discussion

Synthetic procedures: The synthesis of **T1** and **T2** is shown in Scheme 2 and relies on iterative Sonogashira cross-coupling reactions. The bromo-perylene imide **1**, which is one of the key synthons, was prepared by *O*-arylation of the corresponding trisbromo-perylene imide by copper-catalyzed Ullmann reaction, as described previously.[47] Imide **1** was subjected to the first Sonogashira cross-coupling reaction with trimethylsilylacetylene to afford **2** in a yield of 87% using classic conditions for this transformation. The trimethylsilyl protecting group was cleaved by using potassium carbonate and the resulting perylene imide **3** was treated with the known iodo-quaterthiophene-triisopropylsilylacetylene **4**[24] in a second Sonogashira cross-coupling reaction using palladium tetrakis(triphenylphosphine) and copper iodide as the catalytic system to give **5** in a yield of 49%.

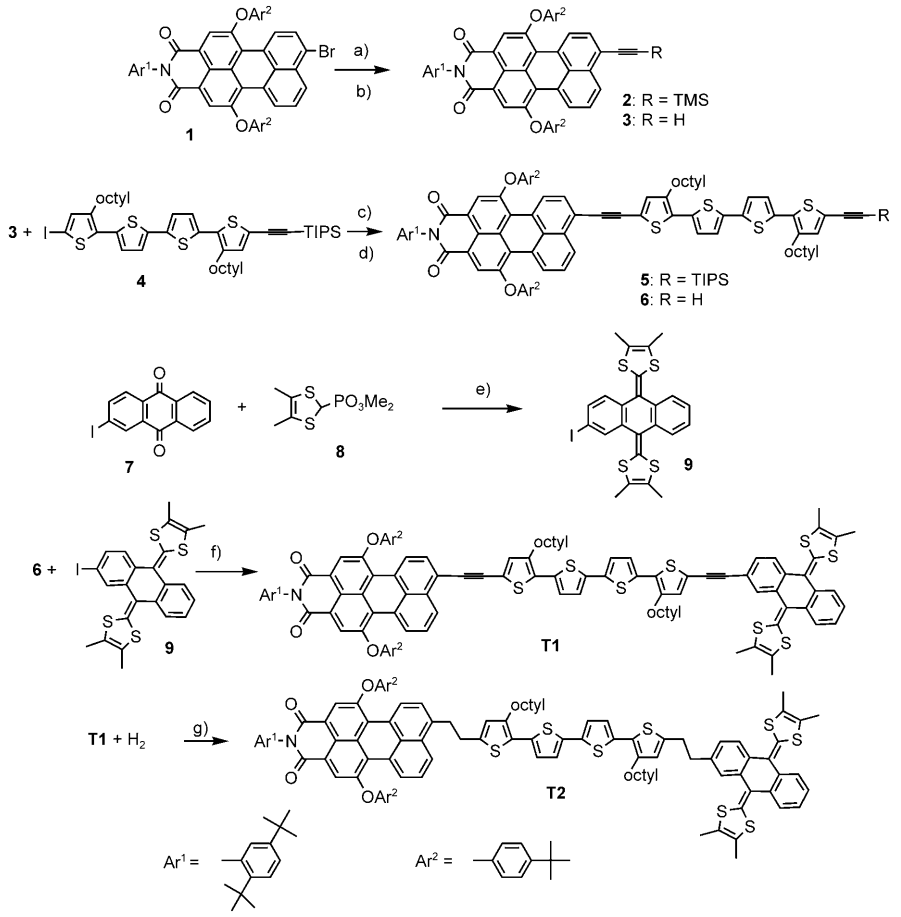

Scheme 2. Preparation of the triads **T1** and **T2**. a) CuI, $[Pd(PPh_3)_2Cl_2]$, trimethylsilylacetylene, toluene, Et_3N, 50 °C (87 %); b) K_2CO_3, CH_2Cl_2, MeOH, RT (100 %); c) CuI, $[Pd(PPh_3)_4]$, THF, Et_3N, 80 °C (49 %); d) Bu_4NF, THF, RT (100 %); e) BuLi, THF, −78 °C (49 %); f) CuI, $[Pd(PPh_3)_4]$, THF, Et_3N, 80 °C (63 %); g) Pd/C, 40 °C (100 %).

Removal of the triisopropylsilyl group with tetrabutylammonium fluoride afforded **6** in an almost quantitative yield. 2-Iodo-9,10-bis(4,5-dimethyl-1,3-dithiol-2-ylidene)-9,10-dihydroanthracene (**9**) was prepared by the Wittig–Horner reaction by condensation of the 2-iodoanthraquinone (**7**) with the carbanion generated from dimethyl (4,5-dimethyl-1,3-dithiol-2-yl)phosphonate (**8**) and butyllithium.[48–50] The resulting iodo-substituted extended TTF **9** was finally grafted onto **6** in the last Sonogashira cross-coupling reaction to afford the first triad **T1** in a yield of 63 % after purification.

The second triad **T2** was obtained by reduction of the triple bonds in triad **T1** under a hydrogen atmosphere using palladium on charcoal as the catalyst (Scheme 2). Note that triad **T2** was systematically contaminated with a small amount of not fully reduced triad (< 15 %), as judged by the presence of a small signal for $[M-2H]^+$ in the mass spectrum of **T2**. The separation of these two compounds was not possible by column chromatography and therefore all the analyses were conducted on the mixture.

The synthesis of dyads **D1** and **D2** is outlined in Scheme 3. It starts with the iodo-quaterthiophene-triisopropylsilylacetylene **4**, which was first capped with phenylacetylene in a Sonogashira cross-coupling reaction to give **10**. Subsequently the triisopropylsilyl protecting group in **10** was cleaved with tetrabutylammonium fluoride and the resulting acetylene **11** was connected to bromo-perylene imide **1** in a second Sonogashira cross-coupling reaction to give **D1**. Dyad **D1** was finally reduced with hydrogen to afford the expected dyad **D2**. The new compounds were satisfactorily characterized by ^1H NMR spectroscopy and high-resolution mass spectrometry

Electronic absorption spectra: Figure 2 shows a superimposition of the spectra of triad **T1** and dyad **D1** along with those of their constituents and the spectroscopic data of the compounds are presented in Table 1.

The spectra of the two compounds **T1** and **D1** are dominated by two broad absorption bands located at around 430 and 560 nm, but each band is composed of several transitions that occur in the different chromophores. The perylene imide dye displays an intense absorption band at around 530 nm, which corresponds to a $\pi\rightarrow\pi^*$ transition, the vibronic bands of which are still visible in the spectrum of trimethylsilylacetylene-perylene imide **2**.[51,52] Quaterthiophene exhibits a broad $\pi\rightarrow\pi^*$ transition at

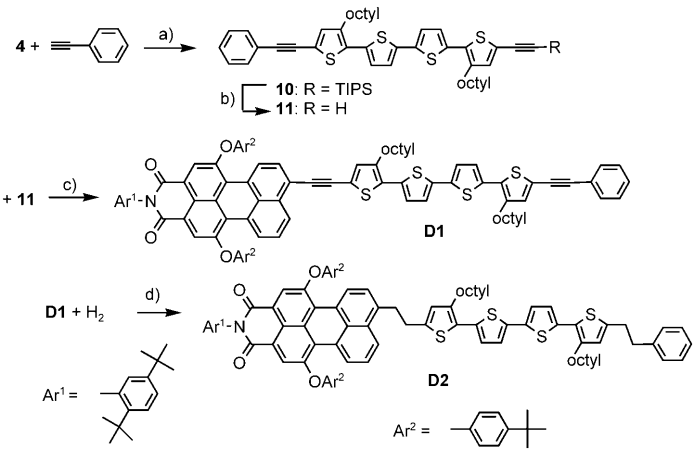

Scheme 3. Preparation of the dyads **D1** and **D2**. a) CuI, $[Pd(PPh_3)_4]$, THF, Et_3N, 80 °C (69 %); b) Bu_4NF, CH_2Cl_2, MeOH, RT (100 %); c) CuI, $[Pd(PPh_3)_4]$, THF, Et_3N, 80 °C (7 %); d) H_2, Pd/C, 40 °C (100 %).

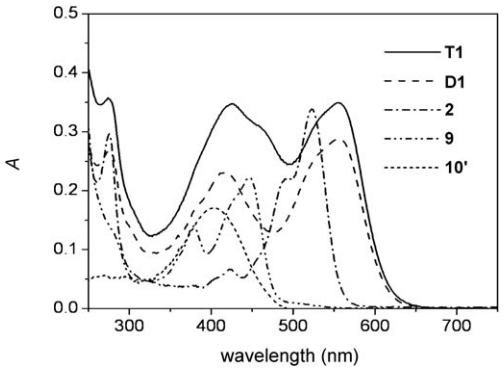

Figure 2. Absorption spectra of dyad **D1**, triad **T1**, and of their molecular components in dichloromethane (absorbance, arbitrary units; molar absorptivity values are given in Table 1). **10′** = 5-(triisopropylsilylethynylene)-5‴-(trimethylsilylethynylene)-3,3‴-dioctyl[2,2′:5′,2″:5″,2‴]quaterthiophene.

Table 1. Characteristics absorption data for the dyads, triads, and molecular components recorded in dichloromethane.

	λ_{abs} [nm] (ε [$M^{-1}cm^{-1}$])
D1	276 (45000), 383 (29000), 418 (39000), 528 (44000), 556 (49000)
D2	274 (42000), 393 (24000), 488 (29000), 519 (33000)
T1	273 (37000), 427 (36000), 464 (32000), 554 (36000)
T2	268 (35000), 399 (20000), 489 (13000), 525 (19000)
2	275 (29000), 494 (22000), 522 (33000)
9	288 (30000), 383 (17000), 430 (19000), 453 (24000)
10′[a]	256 (8600), 289 (5800), 404 (21000)
10″[b]	398 (28000)

[a] **10′** = 5-(Triisopropylsilylethynylene)-5‴-(trimethylsilylethynylene)-3,3‴-dioctyl[2,2′:5′,2″:5″,2‴]quaterthiophene. [b] **10″** = 3,3‴-Dioctyl[2,2′:5′,2″:5″,2‴]quaterthiophene.

around 400 nm located in the same region as those of the extended TTF. The absorption bands of exTTF are also attributed to $\pi \rightarrow \pi^*$ transitions characterized by significant charge transfer from the dithiolium units to the central aromatic core.[36] Clearly the spectra of dyad **D1** and triad **T1** are not a mere linear combination of the spectra of each chromophore. This indicates significant ground-state electronic interactions between each unit in **D1** and **T1**. For example, the absorption band of the parent perylene imide **2**, initially located at 522 nm, is red-shifted, respectively, to 556 and 554 nm in dyad **D1** and triad **T1**.

This shift can be the consequence of a decrease in the HOMO–LUMO gap within the PMI unit as a consequence of increased intercomponent interactions and/or the appearance of a new band arising from charge transfer from the quaterthiophene unit to PMI. Both hypotheses are consistent with DFT calculations (see below). Tails attributed to charge-transfer transitions have previously been observed by Bäuerle and co-workers for perylene imide linked to oligothiophene units.[32–34] The spectrum of triad **T1** differs to that of dyad **D1** first by the enhanced intensity of the band at around 420 nm and secondly by the presence of a shoulder at 464 nm. These changes are brought about by the overlapping contribution of the two transitions of exTTF (Figure 2).

Further clear evidence for ground-state electronic coupling between the units can be found by comparison of the absorption spectra of the two triads **T1** and **T2**, which differ significantly in the larger absorbance in the PMI region for **T1** (Figure 3). In the triad **T1**, there is significant electronic communication between the linked chromophores, which is

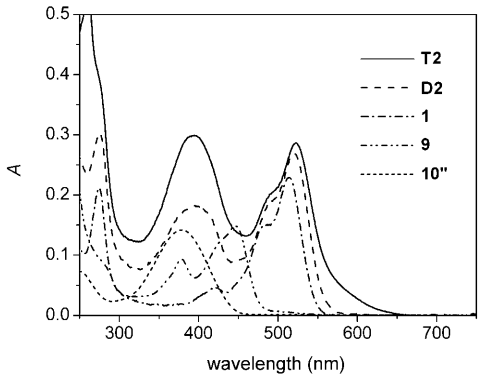

Figure 3. Absorption spectra of dyad **D2**, triad **T2**, and of their molecular components in dichloromethane (absorbance, arbitrary units; molar absorption values are given in Table 1). **10″**.

promoted by the ethynylene linkages that create a π-conjugated pathway throughout the molecule. Conversely, in the triad **T2**, the presence of saturated ethylene linkages between each unit interrupts the conjugation and disrupts the communication between the linked elements. As a result, the three units behave independently and the spectrum of **T2** can be considered as a reasonable sum of the absorbances of each individual chromophore (Figure 3). In the spectrum of triad **T2**, the tail on the red edge of the perylene monoimide absorption band is due to a small amount (from spectral fitting, ca. 15%) of an unsaturated compound that results from the incomplete reduction of **T1** in the synthetic procedure. After repeated attempts at purification by various means (see Synthetic procedures), this impurity proved to be unavoidable.

Electrochemical study: The elementary electron-transfer processes that can take place following excitation of the PMI chromophore in the dyad and triad systems are defined in Scheme 4. To determine the thermodynamic requirements of the various electron-transfer processes, the redox potentials of the units comprising the dyads and triads were determined by cyclic voltammetry and square-wave stripping in dichloromethane. The half-wave potentials are collected in Table 2. The assignments of the redox processes in the dyads and triads were made by comparison with the redox potentials of individual units such as **2**, **9**, and **10′**, which serve as references for PMI, exTTF, and QT, respectively.

The cathodic region shows two reversible reduction processes attributed to the stepwise introduction of an electron

*PMI-QT → PMI^{-}-QT^{+}
charge separation (CS)

PMI^{-}-QT^{+} → PMI-QT
charge recombination (CR)

*PMI-QT-exTTF → PMI^{-}-QT^{+}-exTTF
charge separation (CS)

PMI^{-}-QT^{+}-exTTF → PMI-QT-exTTF
primary charge recombination (CR1)

PMI^{-}-QT^{+}-exTTF → PMI^{-}-QT-exTTF^{+}
hole shift (HS)

PMI^{-}-QT-exTTF^{+} → PMI-QT-exTTF
long-range charge recombination (CR2)

Scheme 4. Elementary electron-transfer processes following excitation of the dyads and triads.

Table 2. Redox potentials of the dyads and triads measured in dichloromethane with 0.15 M of Bu_4NPF_6 as the supporting salt.[a]

	E_{Red2} ($PMI^{1-/2-}$) [V]	E_{Red1} ($PMI^{0/1-}$) [V]	E_{Ox1} ($exTTF^{2+/0}$) [V]	E_{Ox2} ($QT\mathbf{1}^{+/0}$) [V]	E_{Ox3} ($QT\mathbf{2}^{+/1+}$) [V]	E_{Ox4} ($PMI^{1+/0}$) [V]
2	−1.36	−0.95				1.25
9			0.38			
10′				0.94	1.20	
D1	−1.29	−0.93		0.84	1.12	1.37
D2	−1.30	−1.04		0.82	1.05	1.22
T1	−1.26	−0.94	0.42	0.83	1.15	1.37
T2	−1.36	−1.01	0.34	0.80	1.00	1.20

[a] All the potentials are referenced versus the saturated calomel electrode (SCE).

into the perylene monoimide to form PMI^{-} and PMI^{2-}, respectively, in which the spin density is mostly delocalized on the aromatic system of the perylene core (see the molecular orbital representations below). In the unsaturated systems (**D1** and **T1**), these reduction processes are shifted anodically owing to the longer π conjugation through the ethynylene linkages, which induce a stabilization of the LUMO orbitals (see the Computational study section below). Conversely, the inductive effect of the ethylene linkers in **D2** and **T2** makes the PMI more difficult to reduce than the parent compound **2**.

The anodic region exhibits multiple waves because all three units are redox active in the electrochemical window explored under our conditions. In the dyads, the two first one-electron reversible waves at around 0.82 and 1.1 V correspond, respectively, to the formation of the mono- and dication of the quaterthiophene. They are followed by a reversible oxidation reaction located on the PMI at around 1.3 V. The presence of the ethynylene linkage in **D1** raises the energy of the HOMO orbital and also increases the coulombic electrostatic repulsion when several positive charges accumulate in the same molecule. As a consequence, the half-wave potentials are shifted towards more positive values in **D1** with respect to **D2**.

In the triads the additional exTTF unit gives its electrochemical signature at around 0.4 V. Referring to published works reporting the electrochemical properties of exTTF, this wave is attributed to a two-electron process involving the direct transformation of the neutral exTTF into the dication.[36,40,53] The reason for the two-electron process (and for the lack of an intermediate one-electron step) lies in the large stabilization accompanying the transformation of the saddle-shaped neutral molecule, in which the central ring is not aromatic, into a planar anthracenyl system with the 1,3-dithiolium cations lying almost orthogonal to the newly formed aromatic core. At higher potentials, we observe the two stepwise oxidations of quaterthiophene and finally that of PMI.

The potentials measured in the conjugated systems (**D1** and **T1**) differ significantly to those with the saturated linkages (**D2** and **T2**). This confirms the conclusion drawn from the UV/Vis absorption study that there are significant electronic interactions between each unit when they are linked through an ethynylene spacer.

The above redox potentials, together with the absorption and fluorescence spectra, permit the free-energy changes expected for the electron-transfer processes in Scheme 4 to be estimated. The free energy of the various charge-transfer states can be estimated by using the classic Weller formalism given by Equation (1), whereas the energy of the excited singlet state of the PMI unit (E_{00}) can be obtained as an average of the absorption and emission maxima of the dyads and triads, or of model systems thereof. In Equation (1), e is the charge of the electron, ε_0 is the permittivity of a vacuum, R_{DA} is the donor–acceptor center-to-center distance, r^{+} and r^{-} are the radii of the positive and negative ions, ε_s is the dielectric constant of the solvent used (diethyl ether: $\varepsilon_s=4.33$; toluene: $\varepsilon_s=2.38$; dichloromethane: $\varepsilon_s=8.93$), and ε_{ref} is the dielectric constant of the solvent in which the electrochemical data are obtained (in this case, dichloromethane). The R_{DA} distances and the effective radii r^{+} and r^{-} were estimated from DFT-optimized structures (see below and the Supporting Information). The free-energy changes calculated for the electron-transfer processes in Scheme 4 are collected in Table 3.

$$\Delta G(A^{-}D^{+}) = e[E_{ox}(D) - E_{red}(A)] - \frac{e^2}{4\pi\varepsilon_0\varepsilon_s R_{DA}} + \frac{e^2}{8\pi\varepsilon_0}\left(\frac{1}{r^{+}}+\frac{1}{r^{-}}\right)\left(\frac{1}{\varepsilon_s}-\frac{1}{\varepsilon_{ref}}\right) \quad (1)$$

Photophysical study: The photophysical behavior of the dyads and triads was studied by emission and time-resolved absorption techniques in solvents of different polarity. The results will be presented and discussed in some detail for the saturated systems **D2** and **T2**, which are better defined from a supramolecular viewpoint. The unsaturated analogues **D1** and **T1** will be then be discussed on a comparative basis. Detailed experimental results are given in the Supporting Information.

Model PMI: The absorption and emission spectra of the model compound **2** in dichloromethane are shown in Fig-

Table 3. Excited-state energies and free-energy changes[a] associated with the electron-transfer processes presented in Scheme 4.

		Dichloromethane	Diethyl ether	Toluene
	E_{00}	2.31[b]	2.31[b]	2.33
D2	ΔG_{CS}	−0.54	−0.35	−0.05
	ΔG_{CR}	−1.77	−1.960	−2.28
	E_{00}	2.18[b]	2.18[b]	2.12
D1	ΔG_{CS}	−0.50	−0.31	0.07
	ΔG_{CR}	−1.68	−1.87	−2.19
	E_{00}	2.31[b]	2.31[b]	2.30
	ΔG_{CS}	−0.59	−0.40	−0.08
T2	ΔG_{CR1}	−1.72	−1.91	−2.22
	ΔG_{HS}	−0.42	−0.37	−0.34
	ΔG_{CR2}	−1.30	−1.52	−1.88
	E_{00}	2.18[b]	2.18[b]	2.12
	ΔG_{CS}[c]	−0.50	−0.31	0.07
T1	ΔG_{CR1}[c]	−1.68	−1.87	−2.19
	ΔG_{HS}[c]	−0.37	−0.33	−0.29
	ΔG_{CR2}[c]	−1.31	−1.54	−1.90

[a] Calculated from Equation (1). [b] Given the complete quenching of the fluorescence of the PMI unit, the excited-state energy was estimated from the absorption of the dyad/triad and emission from the model system **2**. [c] The physical meaning of these formal labels is limited by the strong delocalization found in this system in the QT–exTTF moiety (see below).

ure 4a. The intense emission with $\lambda_{max}=564$ nm has a quantum yield close to unity and a lifetime of 5.0 ns. The transient difference spectrum of the singlet excited state of PMI, as obtained by ultrafast spectroscopy of **2** in dichloromethane, is shown in Figure 4b. The bleaching observed in the 470–620 nm range with a maximum at around 530 nm is due to a combination of ground-state absorption bleaching and stimulated emission, whereas the positive feature with a maximum at around 730 nm represents an excited-state absorption. As expected on the basis of the emission lifetime, this difference spectrum is manifestly constant in the 1 ns time frame of the ultrafast experiment. No transient was observed in the nanosecond laser photolysis of **2** (timescale >10 ns), which is consistent with high fluorescence efficiency and the negligible intersystem crossing yield of this molecule.

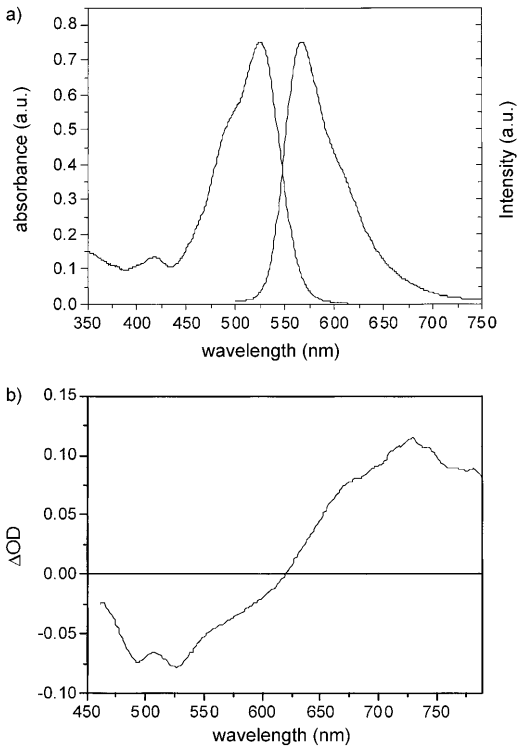

Figure 4. Photophysical properties of PMI model system **2** in dichloromethane. a) Absorption and emission spectra. b) Transient spectrum obtained in ultrafast spectroscopy (excitation at 490 nm); constant in the time window 0–1 ns.

Dyad and triad with saturated linkers

*Dyad **D2***: The energy-level diagram for dyad **D2** in dichloromethane, obtained from spectroscopic and electrochemical data (Table 2), is shown in Figure 5. The energies of the triplet states of the two molecular components have been taken from literature data.[54,55]

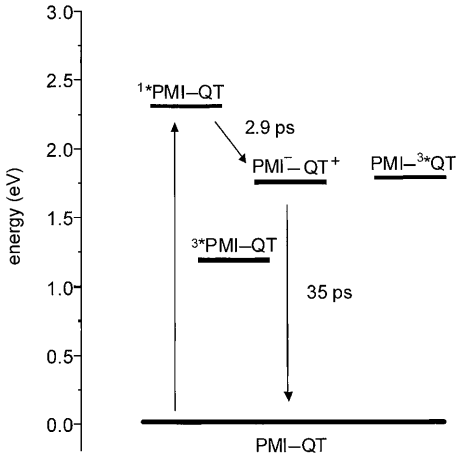

Figure 5. Energy-level diagram for dyad **D2** in dichloromethane.

In dyad **D2** in dichloromethane (dielectric constant, $\varepsilon=8.93$), the emission of the PMI unit is completely quenched.[56] On the basis of the energy-level diagram in Figure 5, the emission quenching is very likely due to photoinduced electron transfer from the QT unit to the excited PMI. Ultrafast spectroscopy (Figure 6) permits direct observation of the process. The first spectrum, taken immediately after the pump pulse, is identical to that of the model system **2** (Figure 4b) and is thus assigned to the S_1 state of the PMI component. It consists of bleaching at $\lambda<600$ nm (bleaching of the ground-state absorption plus some stimulated emission) and of a positive absorption peaking at 660 nm. The transient spectral changes are clearly biphasic. In the first process (Figure 6a), the bleaching corresponding to the PMI ground-state absorption at around 530 nm is essentially maintained, whereas that corresponding to stimulated emission in the 550–650 nm range disappears and the

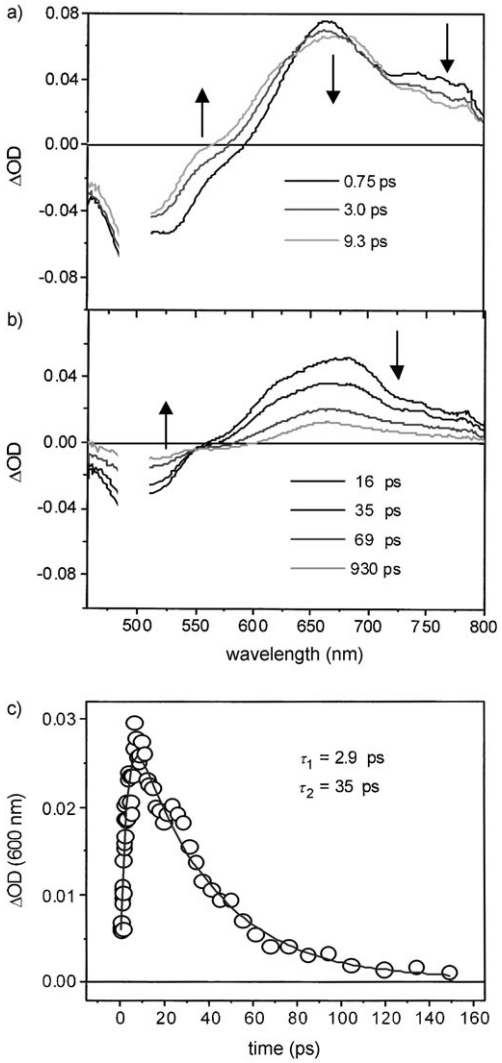

Figure 6. Ultrafast spectroscopy of dyad **D2** in dichloromethane (excitation at 490 nm).

maximum at 660 nm evolves into a broader two-featured profile (maximum at 690 nm, shoulder at 610 nm). These spectral changes are exactly as expected for photoinduced electron transfer based on spectroelectrochemistry observations in which the 610 nm absorption of the PMI radical anion and the 690 nm absorption of the QT radical cation are observed upon reduction and oxidation of the **D2** dyad, respectively (Figure SI1 of the Supporting information). In the second process (Figure 6b), the spectral features of the charge-separated state decay monotonically with isosbestic points close to the baseline, consistent with a charge recombination process leading back to the ground state (the residual absorption, with the same profile as the initial spectrum, is assigned to the same impurity of free PMI observed in emission[56]). The kinetics observed (Figure 6c) agree with standard electron-transfer theory,[57–60] which predicts a very high rate for the moderately exergonic charge-separation step ($\Delta G = -0.54$ eV, likely to be close to the activationless regime) and a lower rate for the highly exergonic charge-recombination step ($\Delta G = -1.77$ eV, likely to lie in the Marcus inverted region).[61] Consistent with the finding that charge recombination leads efficiently to the ground state, no long-lived transient was observed in laser flash photolysis experiments (timescale >10 ns) in dichloromethane. The photophysical behavior of **D2** in dichloromethane is summarized in Figure 5.

In diethyl ether ($\varepsilon = 4.33$), the PMI fluorescence is again completely quenched in the **D2** dyad.[56] The transient spectral changes (Figure SI2) are qualitatively the same as in dichloromethane, with the formation and subsequent decay of a two-peak structure corresponding to the radical ions. The kinetics for the formation (45 ps) and decay (680 ps) of the transient are slower than in dichloromethane. This can be easily explained on the basis of the expected rise in energy of the charge-separated state in the less polar solvent and the consequent changes in the driving force for the charge separation and recombination processes.[62] The former, in the normal free-energy region, is expected to slow down as the driving force decreases, whereas the latter is pushed further into the Marcus inverted region by the increase in the driving force.[63] Again, no long-lived transient was observed in laser flash photolysis experiments (timescale >10 ns) in diethyl ether.

In toluene ($\varepsilon = 2.38$), in contrast to the other solvents, the PMI emission of dyad **D2** is only partially quenched: The lifetime is 3.0 ns and the quantum yield is around 60% of that of the PMI model **2**. Also, the transient behavior (Figure 7) is very different to that observed in the other solvents. The initial spectrum is again that of the singlet excited state of PMI (see Figure SI3), but the spectral changes are qualitatively similar to, but much slower (ca. 2 ns) than those observed initially in the other solvents and no transient decay is observed in the time window (0–1 ns) of the experiment. On a longer timescale, flash photolysis experiments revealed the presence of a long-lived transient (Figure 8) with an oxygen-dependent lifetime (deaerated, 2.6 μs; aerated, 350 ns), which, by comparison with literature data,[55] can be unequivocally assigned to the triplet state of the PMI unit.

The sharply different behavior observed in toluene is very likely determined by the low polarity of this solvent, which raises the charge-separated state to energies comparable to that of the singlet state of the PMI unit (Table 3, Figure 9).[64] In this case, the small fluorescence quenching and the slow transient spectral changes are consistent with the PMI excited singlet state undergoing conversion to (or equilibration with) a charge-separated state, a process with little, if any, driving force. As to the efficient formation of the PMI triplet state observed on the longer timescale, direct S_1 **T1** intersystem crossing within the PMI unit can be ruled out because no triplet state can be observed following excitation of the highly fluorescent model **2**. Therefore a likely mechanism is triplet formation upon charge recombination. For this mechanism to be efficient, the charge-separated state (initially formed by photoinduced electron transfer in a singlet spin state) must be able to undergo spin in-

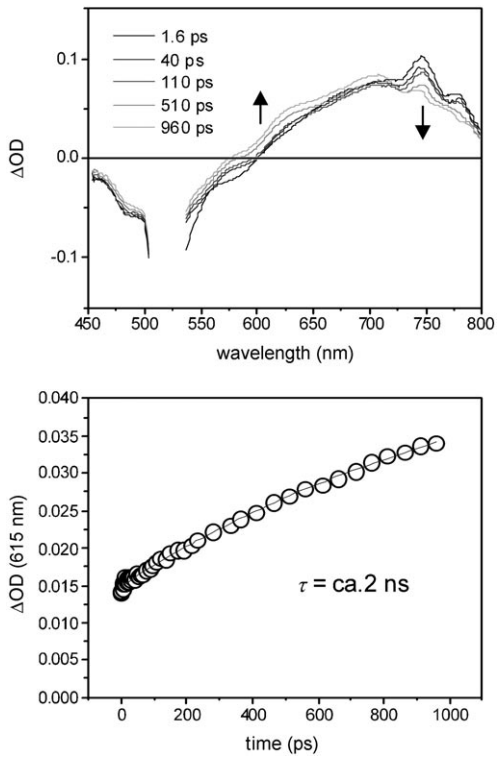

Figure 7. Ultrafast spectroscopy of dyad **D2** in toluene (excitation at 520 nm).

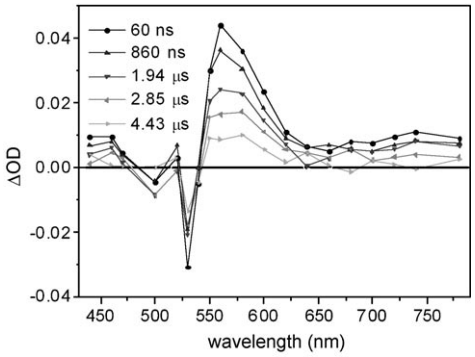

Figure 8. Nanosecond flash photolysis of dyad **D2** in toluene (excitation at 532 nm).

version (intersystem crossing) before recombination. This process can be efficient in toluene because of the intrinsic slowness of the competing spin-allowed recombination to the ground state brought about by its highly exergonic inverted nature. This recombination mechanism in solvents of low polarity is common to other dyad systems involving aromatic imides.[65,66] Whether the PMI triplet is formed directly by charge recombination or by the intermediate formation of the QT triplet followed by fast triplet energy transfer is not possible to determine on the basis of the experimental results. The photophysical behavior of **D2** in toluene is summarized in Figure 9.

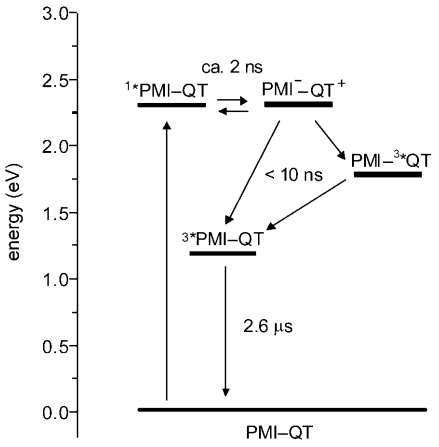

Figure 9. Energy-level diagram for dyad **D2** in toluene.

*Triad **T2***: The energy-level diagram for triad **T2** in dichloromethane, obtained from the spectroscopic and electrochemical data (Table 3), is shown in Figure 10. The only triplet state included in this energy-level diagram is the lowest one, localized on the PMI unit. As for the PMI^{-}–QT–$exTTF^{+}$ charge-separated state, a lower limiting energy value (see discussion in the Computational study section) is indicated by the full line, based on the experimental two-electron oxidation potential of the exTTF unit. For the triad **T2** in dichloromethane, the PMI emission is totally quenched relative to model **2**. Similarly to the corresponding dyad **D2**, the quenching is very likely due to photoinduced electron transfer from the directly linked QT unit. The ultrafast spectroscopy experiments (Figure 11) confirm this assumption. The very fast (1.2 ps) process with bleach recovery in the 550–630 nm range (stimulated emission) and the positive change with the formation of a broad absorption maximum at longer wavelengths (Figure 11a) is attributed to the primary charge-separation step ^{1}*PMI–QT–exTTF→PMI^{-}–QT^{+}–exTTF. The subsequent spectral evolution shows complete

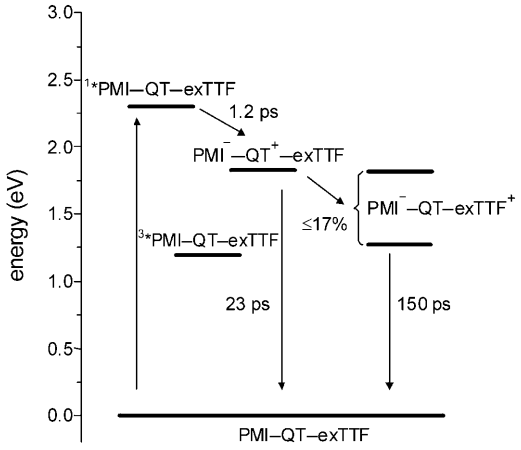

Figure 10. Energy-level diagram for triad **T2** in dichloromethane. For the PMI^{-}–QT–$exTTF^{+}$ charge-separated state, the lower limiting energy value calculated using the experimental $2e^{-}$, oxidation potential of exTTF is shown (full line; see text).

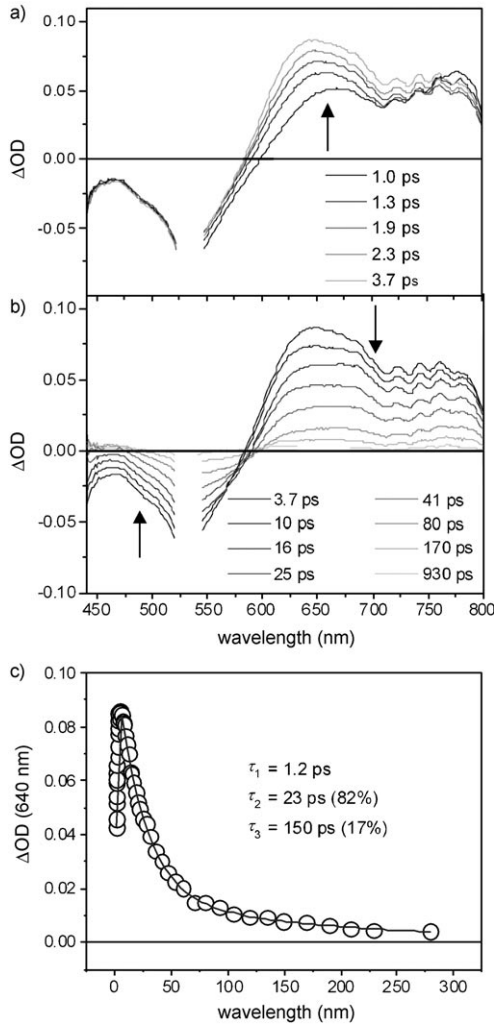

Figure 11. Ultrafast spectroscopy of triad **T2** in dichloromethane (excitation at 530 nm).

decay of the spectral changes back to the baseline (Figure 11b). The process is not a simple one, as indicated by the lack of a clear isosbestic point and by the biexponential kinetics (Figure 11c) but, overall, it is remarkably similar to that observed for dyad **D2**. This suggests that the decay of the primary charge-separated state involves as the main process fast (23 ps) charge recombination to the ground state (PMI^{-}–QT^{+}–exTTF→PMI–QT–exTTF). Note, however, that clear spectroscopic discrimination between primary (PMI^{-}–QT^{+}–exTTF) and long-range (PMI^{-}–QT–$exTTF^{+}$) charge-separated states is difficult because of the largely similar signatures expected for the radical cations of QT ($\lambda_{max}=690$ nm, Figure SI1) and exTTF ($\lambda_{max}=680$ nm[41]). Therefore the occurrence of some charge shift (PMI^{-}–QT^{+}–exTTF→PMI^{-}–QT–$exTTF^{+}$) in competition with the main primary charge recombination process cannot be ruled out. In this hypothesis, the minor, longer-lived (150 ps) component of the overall decay can be tentatively associated with a long-range recombination process. The yield of this process can be estimated from the weight of the slow component (17%) assuming similar molar absorption coefficients of the primary and long-range charge-separated states at the examined wavelength. The strong similarity between the behavior of triad **T2** and that observed for dyad **D2** is maintained in solvents of lower polarity. In diethyl ether, the recombination of PMI occurs in the short ps timescale and leads again to the triplet state of the PMI unit (Figure SI5).

Dyad and triad with unsaturated linkers

*Dyad **D1***: The photophysical behavior of dyad **D1** is qualitatively similar to that described above for **D2**. In particular, complete quenching of the PMI emission is observed in dichloromethane and diethyl ether, whereas only partial quenching is observed in toluene. The transient spectral changes of **D1** (Figure 12) are again biphasic and indicate the occurrence of charge separation and recombination with the eventual formation of ground-state products in dichloromethane and diethyl ether and of the PMI triplet state in toluene (Figure SI6). Differences with respect to **D2** (e.g., in the spectral shape of emission and transient absorption) can be traced back to the previously mentioned large intercomponent interaction taking place in the dyad across the unsaturated ethynylene linkage. In particular, the emission observed in toluene, which is significantly red-shifted and much broader than that of the PMI model **2** and dyad **D2** (Figure SI7), can be attributed to a strongly perturbed PMI fluorescence or, alternatively, to a new emission with charge-transfer characteristics. The appreciable delocalization of the MOs of PMI and QT on the neighboring unit in **D1**, as indicated by the DFT calculations (see below), indicates that, indeed, emission from the PMI^{-}–QT^{+} charge-separated state may have appreciable oscillator strength. Charge-transfer emission has previously been observed by De Schryver and co-workers in a directly linked PMI-bisthiophene dyad.[34]

*Triad **T1***: In line with the observations made for the dyad systems, the behavior of the unsaturated triad **T1** is rather similar to that of the saturated analogue **T2**. The transient spectral changes observed in dichloromethane are shown in Figure 13. Again, after a very fast (Figure 13a, 1.4 ps, inset Figure 13c) process similar to that exhibited by the corresponding dyad and attributed to charge separation, a two-component decay (major time constant 26 ps, minor time constant 160 ps, Figure 13b,c) restores the original baseline. As for the saturated analogue, it is likely that the main recombination path is similar to that of the dyad, that is, fast recombination to the ground state with any other processes constituting, at best, a minor pathway. The solvent effects, including the efficient formation of triplet PMI in toluene (Figure SI8), also follow closely those observed for **T2**.

Energy levels: Computational study: Overall, the results obtained with the triads are somewhat deceiving as the primary charge-separated state seems to recombine largely by primary charge recombination with no substantial gain in

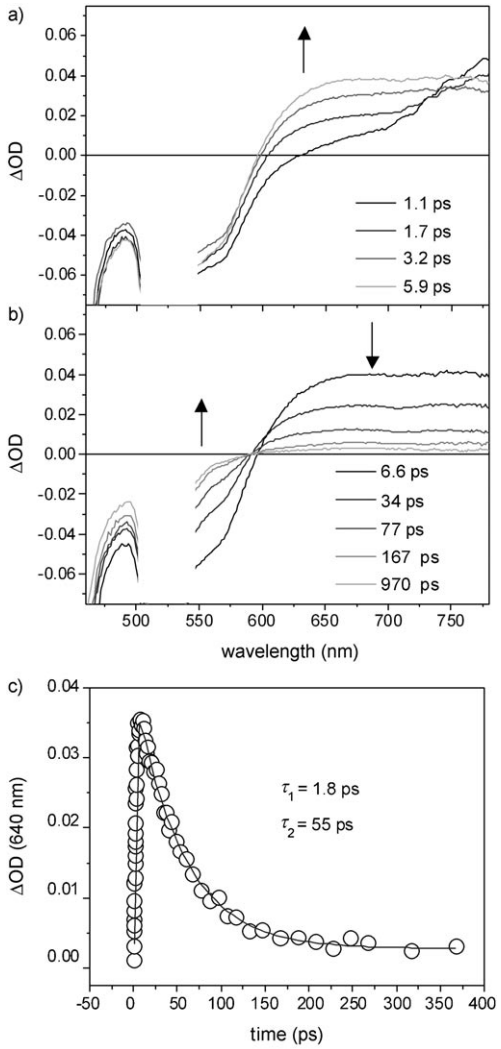

Figure 12. Ultrafast spectroscopy of dyad **D1** in dichloromethane (excitation at 530 nm).

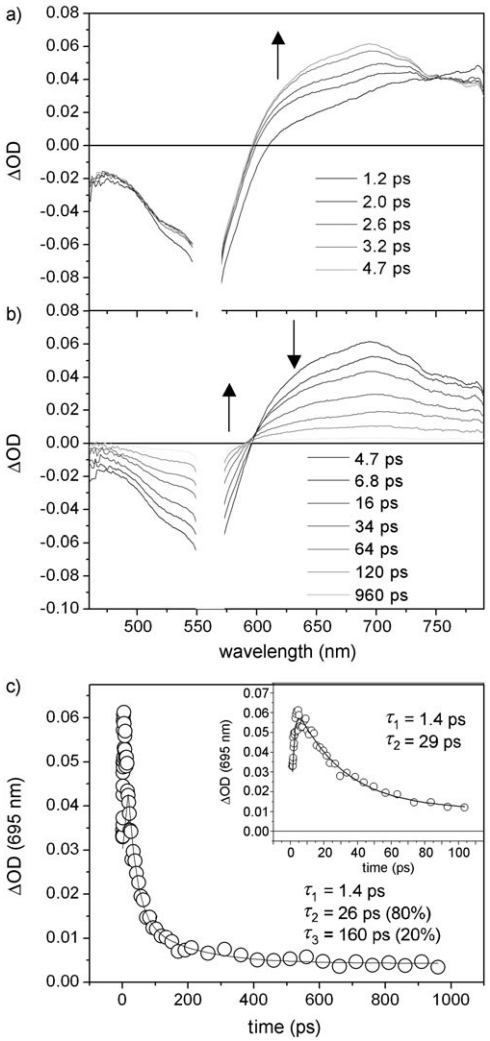

Figure 13. Ultrafast spectroscopy of triad **T1** in dichloromethane (excitation at 560 nm).

charge-separation lifetime with respect to the dyads. This may be surprising considering the almost ideal driving force (ca. 0.4 eV) estimated for charge shift in both **T2** and **T1** (Figure 10 and Table 3). Given the similar driving force and the identical spacers involved, charge shift is expected to be as fast as primary charge separation (few ps), that is, should be able to compete effectively with the slower primary charge recombination process. This not being the case seems to point to a fundamental problem in the evaluation of the energetics of the triads. In fact, it should be kept in mind that the energy of the long-range charge-separated state in Table 3 and Figure 10 was calculated, as usual,[67] by using, faute de mieux, the experimental two-electron oxidation potential of the exTTF unit. The fact that only a two-electron oxidation is experimentally observed for this unit is attributed to the strong stabilization (gain in aromaticity) experienced by the dication upon planarization of the central polyacenic moiety.[68] Thus, the one-electron oxidation potential of exTTF is not known, except for the fact that it must be equal or higher than the experimental two-electron value. The observed disproportionation of the radical monocation, generated radiolytically[69] or by flash photolysis,[41] strongly suggests that the one-electron oxidation potential must be higher than the experimental two-electron value. This is an example of "potential inversion", a phenomenon extensively studied by Evans[70] in organic molecules undergoing structural change coupled with electron transfer. In appropriate cases, the extent of potential inversion (the difference between the first and second redox potentials) can be estimated by voltammetry or by EPR measurement of the comproportionation equilibrium. For exTTF, a lower limit of 0.28 V, determined by voltammetry, was confirmed by quantitative EPR measurements.[71] Interestingly, in cyclophane-type derivatives of exTTF, in which planarization of the dication oxidation is prevented by steric constraints, two stepwise one-electron oxidation processes are observed and the radical cation can be electrochemically generated and spectroscopically characterized.[72] Thus, because of the above-mentioned

problems, the energetics of the triads estimated from electrochemical data are intrinsically uncertain. In an attempt to circumvent the experimental problem, and possibly to understand the reasons for inefficient charge shift, we performed the DFT computational work described below.

Calculations on the electronic ground state of the dyad (**D1** and **D2**) and triad (**T1** and **T2**) model systems were carried out by using the B3LYP functional within the density functional theory method.[73–75] The "pruned" molecular models were tailored for the computational study (aryl and aliphatic substituents replaced with phenyl and methyl residues, respectively) to reduce complexity and cost while still providing a reliable description of the molecular systems investigated experimentally. The geometry (see Figure SI9; the coordinates are presented in the Supporting Information) was fully optimized, without symmetry constraints, by describing the systems with a Dunning–Huzinaga valence "double-ζ" quality basis set.[76] Single-point energy calculations with the standard basis set 6-31G**[77–83] were accomplished to account for the polarization effects. Additional calculations on **T2** were performed to include the solvent effect using the polarizable continuum model[84] (PCM) to simulate dichloromethane ($\varepsilon = 8.93$), that is, the solvent used to collect the spectra of the present molecular systems. All calculations were performed by using the Gaussian 03 software package.[85]

The MO energy diagrams attained at the DFT level for dyads **D1** and **D2** are shown in Figure 14, with each MO labeled by the prominent localization on the system. Whereas for the saturated dyad **D2** the MOs, including the frontier orbitals, are strongly localized on either the PMI or QT units, the unsaturated system exhibits a larger degree of delocalization through the ethynylene spacers. Thus, the frontier orbitals in **D1**, although still being predominantly localized on either the PMI or QT unit, also have significant amplitudes on the neighboring unit. The calculated relative energies of the MOs are consistent with the spectroscopic data for the dyads (Figures 2 and 3), in which the PMI absorption (HOMO-1→LUMO transition) is red-shifted in **D1** relative to **D2**, and the electrochemical data for the dyads (Table 2), with **D1** easier to reduce but more difficult to oxidize than **D2**. In very much the same way, Figure 15 shows the MO energy diagrams for triads **T1** and **T2**. As observed for the dyads, the unsaturated linkers between fragments allow efficient π conjugation and therefore delocalization of the MOs in the case of **T1**. As for the dyads, this is reflected by stationary absorption spectroscopy (Figures 2 and 3) in which the PMI region of the spectra is strongly influenced by the degree of ground-state electronic coupling between the units.

The calculated energy-level diagrams are also valuable in interpreting the photophysical results. For the dyads, Figure 14 clearly shows that the lowest excited state (corresponding to the HOMO→LUMO transition) is a PMI^{-}–QT^{+} charge-separated state and that the driving force for populating such a state from the PMI local excited state is large (to a first approximation, the HOMO–HOMO-1 energy difference). These findings are fully consistent with the very fast charge separation observed for both dyads in dichloromethane.

The most interesting result relates to the triads, however. In the energy-level diagram of **T2** (Figure 15) it is clearly

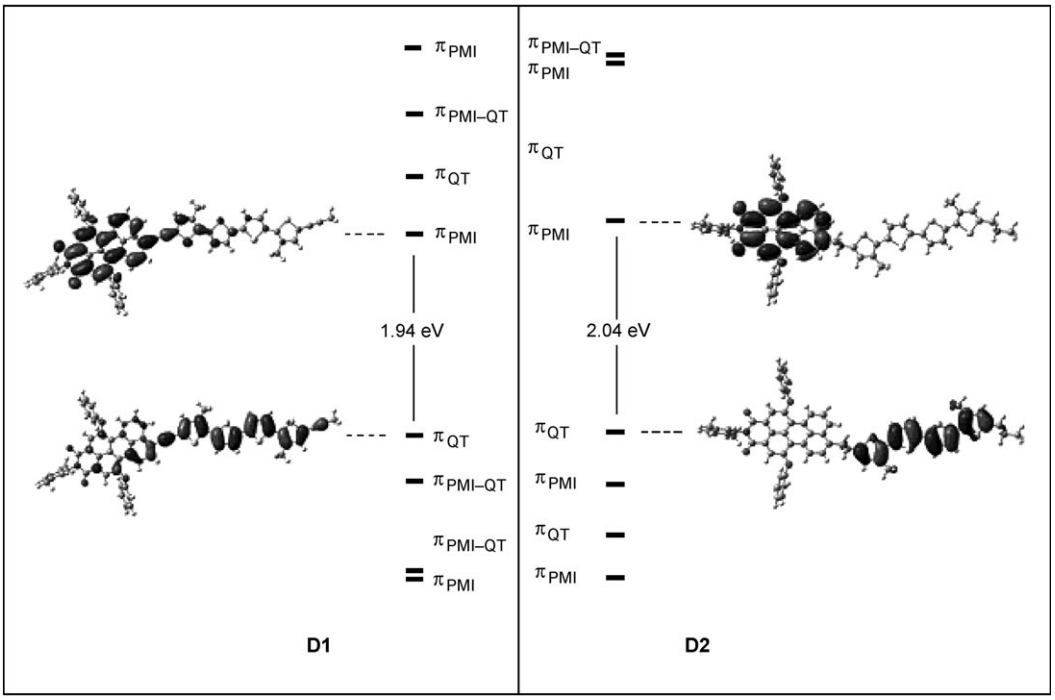

Figure 14. MO energy diagrams of the dyads **D1** and **D2** calculated in the gas phase at the B3LYP/6-31G** level of theory, along with HOMO and LUMO contour plots.

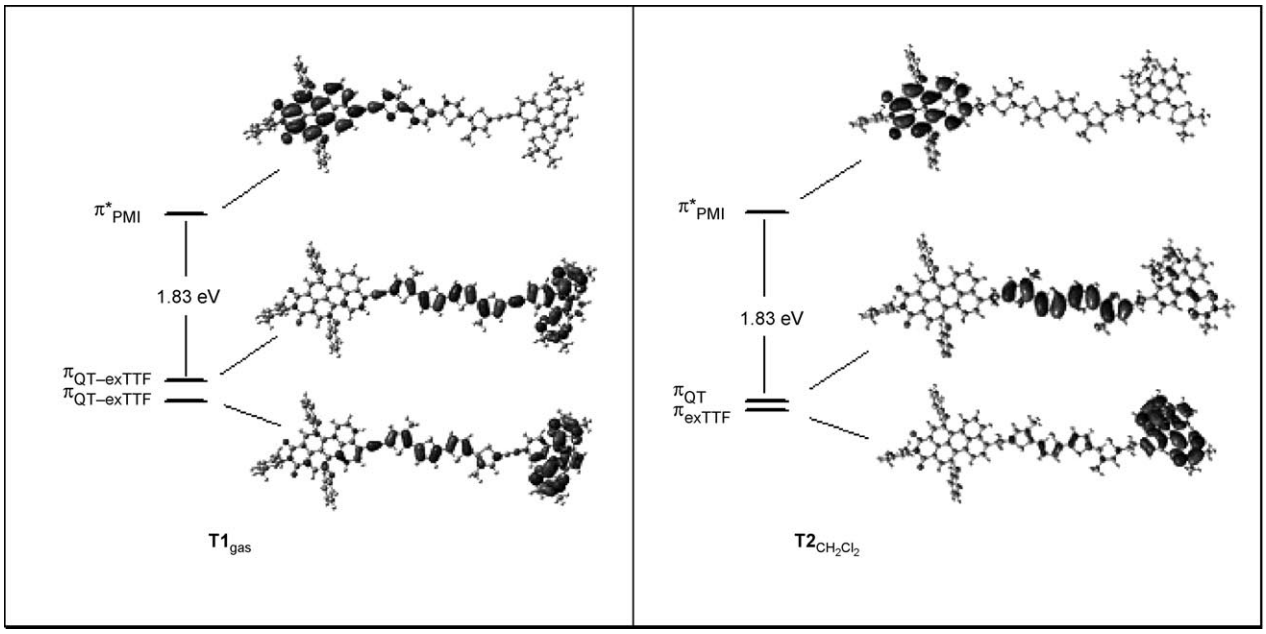

Figure 15. MO energy diagram of the triads **T1** (gas phase) and **T2** (dichloromethane) calculated at the B3LYP/6-31G** level of theory, along with LUMO, HOMO, and HOMO-1 contour plots.

seen that the highest-occupied MOs are a pair of very closely spaced orbitals, one localized on QT and the other on the exTTF unit. The two orbitals are quasi-degenerate, with π_{QT} slightly higher than π_{exTTF} in dichloromethane (quasi-degenerate also in the gas phase, but in the reverse order). The similar energies of the two orbitals imply that the unknown one-electron potential for the oxidation of the exTTF unit must be similar to that of the QT unit, that is, substantially higher (by ca. 0.4 V) than the experimental two-electron potential (Table 2) so that the driving force for charge shift in triad **T2** in dichloromethane must be, if any, very small. The energy state schematized by the dashed level in Figure 10 accounts for the experimental finding that the primary charge-separated state deactivates largely by charge recombination rather than by charge shift and the fact that the minor decay component, attributed to long-range charge recombination, is only moderately slower than the primary process (a two-step process through the almost isoenergetic QT unit is expected to be much faster than a direct transformation).

The results for **T1** show again the presence of two closely spaced highest-occupied MOs. The main difference with respect to the saturated triad lies in the strong delocalization of both orbitals on the QT and exTTF units. Note that the extent of delocalization between neighboring units through the ethynylene linkages is much greater between QT and exTTF (Figure 15) than between PMI and QT (see, for example, the corresponding dyad in Figure 14). In terms of through-bond perturbation, this can be explained by the smaller energy difference between the interacting orbitals of the QT–exTTF fragment relative to PMI–QT. From the photophysical point of view, the strong delocalization in the QT–exTTF fragment suggests that for **T1** some of the terms used in the above discussion should be reconsidered. In particular, the picture of two distinct charge-separated states (primary and long-range) is inappropriate and should be replaced by that of two charge-separated states containing a reduced PMI unit and a collectively oxidized QT–exTTF fragment.

Conclusion

Two dyad and triad systems of the PMI–QT and PMI–QT–exTTF type, differing in the saturated (ethylene) or unsaturated (ethynylene) nature of the linker groups, have been designed, synthesized, and characterized electrochemically, photophysically, and computationally. All the experimental results indicate that, although the saturated systems have weakly interacting, essentially unperturbed molecular subunits (i.e., are strictly supramolecular in nature), in the unsaturated systems strong intercomponent interactions lead to substantial perturbation of the properties of the subunits. The DFT study on **D2** and **T2** indicates MOs largely localized within the molecular components, whereas for **D1** and **T1** more or less extensive delocalization of the MOs over neighboring units takes place across the ethynylene linkers. In **T1**, the delocalization is particularly effective between the QT and exTTF units, which should be more appropriately viewed combined as a single electronic subsystem. This implies that for **T1** the definition of "triad", as well as notions such as charge shift and primary versus long-range charge separation and recombination, lose much of their meaning.

For the dyad systems, the photophysics observed following excitation of the PMI unit is solvent-dependent. In moderately polar solvents, such as dichloromethane and diethyl ether, fast charge separation is followed by recombination to the ground state. In the less polar toluene, slow conversion to (or equilibration with) the charge-separated state is followed by intersystem crossing and recombination to yield the triplet state of the PMI unit. This difference in behavior is related to the solvent effect on the energy of the charge-separated states.

The behavior of the triads is remarkably similar to that of the corresponding dyads, with only minor differences. This indicates that, after primary charge separation, the charge shift to yield a long-range charge-separated state is quite inefficient. At first sight, this result was surprising given the large driving force calculated for charge shift from the electrochemical data. In fact, the problem lies in the electrochemistry of exTTF for which, because of the strong gain in aromaticity achieved in forming the dicationic species, only a single two-electron oxidation process is observed. The matter is clarified by DFT calculations on triad **T2**, which show that, although from electrochemistry exTTF looks much easier to oxidize than QT, the highest-occupied MOs (one-electron redox orbitals) of the two units are almost degenerate. Such a result quantifies the potential inversion[70] of exTTF at around +0.4 V. This value may be of interest for the design of charge-separation systems that include this type of unit, particularly when small driving forces are relevant.[86]

Acknowledgements

The authors would like to thank Maria Teresa Indelli for the critical reading of the manuscript and Roberto Argazzi for precious help with the nanosecond laser photolysis experiments. The Agence Nationale de la Recherche (ANR) is gratefully acknowledged for financial support (program "PhotoCumElec") and the European Community through COST D35 program. Financial support from the Italian MIUR (Grants FIRB RBNE019H9K and PRIN 2006030320) is also gratefully acknowledged.

[1] V. Balzani, A. Credi, M. Venturi, *ChemSusChem* **2008**, *1*, 26–58.
[2] Y. Kobori, S. Yamauchi, K. Akiyama, S. Tero-Kubota, H. Imahori, S. Fukuzumi, J. R. Norris Jr. , *Proc. Natl. Acad. Sci. USA* **2005**, *102*, 10017–10022.
[3] D. A. Lavan, J. N. Cha, *Proc. Natl. Acad. Sci. USA* **2006**, *103*, 5251–5255.
[4] I. M. Bennett, H. M. Farfano, F. Bogani, A. Primak, P. A. Liddell, L. Otero, L. Sereno, J. J. Silber, A. L. Moore, T. A. Moore, D. Gust, *Nature* **2002**, *420*, 398–401.
[5] M. Hambourger, G. F. Moore, D. M. Kramer, D. Gust, A. L. Moore, T. A. Moore, *Chem. Soc. Rev.* **2009**, *38*, 25–35.
[6] T. Otsubo, Y. Aso, K. Takimiya, *J. Mater. Chem.* **2002**, *12*, 2565–2575.
[7] L. Sánchez, M. A. Herranz, N. Martin, *J. Mater. Chem.* **2005**, *15*, 1409–1421.
[8] N. Martin, L. Sanchez, M. A. Herranz, B. Illescas, D. M. Guldi, *Acc. Chem. Res.* **2007**, *40*, 1015–1024.
[9] V. Balzani, P. Piotrowiak, M. A. J. Rodgers, J. Mattay, D. Astruc, H. B. Gray, J. Winkler, S. Fukuzumi, T. E. Mallouk, Y. Haas, A. P. de Silva, I. Gould, *Electron Transfer in Chemistry*, Wiley-VCH, Weinheim, **2001**.
[10] V. Balzani, F. Scandola, *Supramolecular Photochemistry*, Ellis Horwood, Chischester, **1991**.
[11] D. Gust, T. A. Moore, A. L. Moore, *Acc. Chem. Res.* **1993**, *26*, 198–205.
[12] M. R. Wasielewski, *Chem. Rev.* **1992**, *92*, 435–461.
[13] E. Baranoff, J. P. Collin, L. Flamigni, J. P. Sauvage, *Chem. Soc. Rev.* **2004**, *33*, 147–155.
[14] D. M. Guldi, *Pure Appl. Chem.* **2003**, *75*, 1069–1075.
[15] D. M. Guldi, H. Imahori, K. Tamaki, Y. Kashiwagi, H. Yamada, Y. Sakata, S. Fukuzumi, *J. Phys. Chem. A* **2004**, *108*, 541–548.
[16] A. Harriman, J. P. Sauvage, *Chem. Soc. Rev.* **1996**, *25*, 41.
[17] M. R. Wasielewski, *J. Org. Chem.* **2006**, *71*, 5051–5066.
[18] A. Osuka, S. Marumo, N. Mataga, S. Taniguchi, T. Okada, I. Yamazaki, Y. Nishimura, T. Ohno, K. Nozaki, *J. Am. Chem. Soc.* **1996**, *118*, 155–168.
[19] A. Petrella, J. Cremer, C. L. De, P. Bauerle, R. M. Williams, *J. Phys. Chem. A* **2005**, *109*, 11687–11695.
[20] A. Marcos Ramos, E. H. A. Beckers, T. Offermans, S. C. J. Meskers, R. A. J. Janssen, *J. Phys. Chem. A* **2004**, *108*, 8201–8211.
[21] M. Holzapfel, C. Lambert, *J. Phys. Chem. C* **2008**, *112*, 1227–1243.
[22] C. Lambert, J. Schelter, T. Fiebig, D. Mank, A. Trifonov, *J. Am. Chem. Soc.* **2005**, *127*, 10600–10610.
[23] J. Fortage, J. Boixel, E. Blart, L. Hammarstrom, H. C. Becker, F. Odobel, *Chem. Eur. J.* **2008**, *14*, 3467–3480.
[24] J. Fortage, J. Boixel, E. Blart, H. C. Becker, F. Odobel, *Inorg. Chem.* **2009**, *48*, 518–526.
[25] J. Fortage, E. Goransson, E. Blart, H. C. Becker, L. Hammarstrom, F. Odobel, *Chem. Commun.* **2007**, 4629–4631.
[26] T. Nakamura, J. Y. Ikemoto, M. Fujitsuka, Y. Araki, O. Ito, K. Takimiya, Y. Aso, T. Otsubo, *J. Phys. Chem. B* **2005**, *109*, 14365–14374.
[27] T. Nakamura, H. Kanato, Y. Araki, O. Ito, K. Takimiya, T. Otsubo, Y. Aso, *J. Phys. Chem. A* **2006**, *110*, 3471–3479.
[28] H. Kanato, K. Takimiya, T. Otsubo, Y. Aso, T. Nakamura, Y. Araki, O. Ito, *J. Org. Chem.* **2004**, *69*, 7183–7189.
[29] T. Nakamura, M. Fujitsuka, Y. Araki, O. Ito, J. Ikemoto, K. Takimiya, Y. Aso, T. Otsubo, *J. Phys. Chem. B* **2004**, *108*, 10700–10710.
[30] F. Würthner, *Chem. Commun.* **2004**, 1564–1579.
[31] A. Morandeira, J. Fortage, T. Edvinsson, L. Le Pleux, E. Blart, G. Boschloo, A. Hagfeldt, L. Hanmiarstrom, F. Odobel, *J. Phys. Chem. C* **2008**, *112*, 1721–1728.
[32] J. Cremer, P. Bäuerle, *Eur. J. Org. Chem.* **2005**, 3715–3723.
[33] J. Cremer, E. Mena-Osteritz, N. G. Pschierer, K. Mullen, P. Bäuerle, *Org. Biomol. Chem.* **2005**, *3*, 985–995.
[34] E. Fron, M. Lor, R. Pilot, G. Schweitzer, H. Dincalp, F. S. De, J. Cremer, P. Bäuerle, K. Mullen, A. M. Van der, F. C. De Schryver, *Photochem. Photobiol. Sci.* **2005**, *4*, 61–68.
[35] C. Atienza-Castellanos, M. Wielopolski, D. M. Guldi, P. C. van der Pol, M. R. Bryce, S. Filippone, N. Martin, *Chem. Commun.* **2007**, 5164–5166.
[36] M. C. Díaz, B. M. Illescas, C. Seoane, N. Martin, *J. Org. Chem.* **2004**, *69*, 4492–4499.
[37] S. S. Gayathri, M. Wielopolski, E. M. Perez, G. Fernandez, L. Sanchez, R. Viruela, E. Orti, D. M. Guldi, N. Martin, *Angew. Chem.* **2009**, *121*, 829–834; *Angew. Chem. Int. Ed.* **2009**, *48*, 815–819.
[38] F. Giacalone, J. L. Segura, N. Martin, D. M. Guldi, *J. Am. Chem. Soc.* **2004**, *126*, 5340–5341.
[39] F. Giacalone, J. L. Segura, N. Martin, J. Ramey, D. M. Guldi, *Chem. Eur. J.* **2005**, *11*, 4819–4834.
[40] S. González, N. Martin, D. M. Guldi, *J. Org. Chem.* **2003**, *68*, 779–791.
[41] D. M. Guldi, L. Sanchez, N. Martin, *J. Phys. Chem. B* **2001**, *105*, 7139–7144.
[42] S. Romain, J. C. Lepretre, J. Chauvin, A. Deronzier, M. N. Collomb, *Inorg. Chem.* **2007**, *46*, 2735–2743.
[43] R. Konduri, N. R. de Tacconi, K. Rajeshwar, F. M. MacDonnell, *J. Am. Chem. Soc.* **2004**, *126*, 11621–11629.
[44] L. Hammarstrom, *Curr. Opin. Chem. Biol.* **2003**, *7*, 666–673.

[45] F. Odobel, M. Severac, Y. Pellegrin, E. Blart, C. Fosse, C. Cannizzo, C. R. Mayer, K. J. Elliott, A. Harriman, *Chem. Eur. J.* **2009**, *15*, 3130–3138.
[46] A. Harriman, K. J. Elliott, M. A. H. Alamiry, L. Le Pleux, M. Severac, Y. Pellegrin, E. Blart, C. Fosse, C. Cannizzo, C. R. Mayer, F. Odobel, *J. Phys. Chem. C* **2009**, *113*, 5834–5842.
[47] J. Fortage, M. Severac, C. Houarner-Rassin, Y. Pellegrin, E. Blart, F. Odobel, *J. Photochem. Photobiol. A* **2008**, *197*, 156–169.
[48] A. J. Moore, M. R. Bryce, *J. Chem. Soc. Perkin Trans. 1* **1991**, 157–168.
[49] G. J. Marshallsay, M. R. Bryce, *J. Org. Chem.* **1994**, *59*, 6847–6849.
[50] A. J. Moore, M. R. Bryce, A. S. Batsanov, J. C. Cole, J. A. K. Howard, *Synthesis* **1995**, 675–682.
[51] M. Adachi, Y. Nagao, *Chem. Mater.* **2001**, *13*, 662–669.
[52] M. Adachi, Y. Nagao, *Chem. Mater.* **1999**, *11*, 2107–2114.
[53] A. E. Jones, C. A. Christensen, D. F. Perepichka, A. S. Batsanov, A. Beeby, P. J. Low, M. R. Bryce, A. W. Parker, *Chem. Eur. J.* **2001**, *7*, 973–978.
[54] K. Matsumoto, M. Fujitsuka, T. Sato, S. Onodera, O. Ito, *J. Phys. Chem. B* **2000**, *104*, 11632–11638.
[55] R. T. Hayes, C. J. Walsh, M. R. Wasielewski, *J. Phys. Chem. A* **2004**, *108*, 3253–3260.
[56] In fact a small residual emission (intensity, ca. 10% of that of the model) is observed. On the basis of its unquenched lifetime (5 ns), this emission is attributed to an impurity of free PMI.
[57] J. Jortner, *J. Chem. Phys.* **1976**, *64*, 4860–4867.
[58] J. Ulstrup, *Charge Transfer Processes in Condensed Media*, Springer, Berlin, **1979**.
[59] R. A. Marcus, N. Sutin, *Biochim. Biophys. Acta Rev. Bioenerg.* **1985**, *811*, 265–322.
[60] J. R. Miller, J. V. Beitz, R. K. Huddleston, *J. Am. Chem. Soc.* **1984**, *106*, 5057–5068.
[61] With the appropriate parameters (see the Supporting Information), the solvent contribution to the reorganizational energy is estimated to be about 0.6 eV in dichloromethane.
[62] The energy of the charge-separated state in diethyl ether can be estimated by using Equation (1) (using appropriate effective ionic radii, see the Supporting Information) to be ca. 1.96 eV.
[63] Note that a decrease in solvent polarity does not only increase the energy of the charge-separated state, but it also decreases the reorganizational energy of the processes. In the inverted region, the two factors act synergistically to reduce the rates, whereas in the normal regime partial compensation between the two effects should be expected.
[64] The energy of the charge-separated state in toluene can be estimated by using Equation (1) (using appropriate effective ionic radii, see the Supporting Information) to be ca. 2.29 eV.
[65] M. Ghirotti, C. Chiorboli, C. C. You, F. Wurthner, F. Scandola, *J. Phys. Chem. A* **2008**, *112*, 3376–3385.
[66] R. T. Hayes, M. R. Wasielewski, D. Gosztola, *J. Am. Chem. Soc.* **2000**, *122*, 5563–5567.
[67] a) M. C. Díaz, M. A. Herranz, B. M. Illescas, N. Martin, N. Godbert, M. R. Bryce, C. P. Luo, A. Swartz, G. Anderson, D. M. Guldi, *J. Org. Chem.* **2003**, *68*, 7711–7721; b) C. Atienza, N. Martin, M. Wielopolski, N. Haworth, T. Clark, D. M. Guldi, *Chem. Commun.* **2006**, 3202–3204.
[68] N. Martín, L. Sanchez, C. Seoane, E. Orti, P. M. Viruela, R. Viruela, *J. Org. Chem.* **1998**, *63*, 1268–1279.
[69] A. E. Jones, C. A. Christensen, D. F. Perepichka, A. S. Batsanov, A. Beeby, P. J. Low, M. R. Bryce, A. W. Parker, *Chem. Eur. J.* **2001**, *7*, 973–978.
[70] D. H. Evans, *Chem. Rev.* **2008**, *108*, 2113–2144.
[71] N. E. Gruhn, N. A. Macías-Ruvalcaba, D. H. Evans, *Langmuir* **2006**, *22*, 10683.
[72] C. A. Christensen, A. S. Batsanov, M. R. Bryce, *J. Am. Chem. Soc.* **2006**, *128*, 10484–10490.
[73] A. D. Becke, *J. Chem. Phys.* **1993**, *98*, 5648–5652.
[74] P. J. Hay, *J. Phys. Chem. A* **2002**, *106*, 1634–1641.
[75] C. T. Lee, W. T. Yang, R. G. Parr, *Phys. Rev. B* **1988**, *37*, 785–789.
[76] "Gaussian Basis Sets for Molecular Calculations": T. H. J. Dunning, P. J. Hay in *Methods of Electronic Structure Theory* (Ed.: H. F. I. Schaefer), Plenum Press, New York, **1977**.
[77] R. Ditchfield, W. J. Hehre, J. A. Pople, *J. Chem. Phys.* **1971**, *54*, 724–728.
[78] M. S. Gordon, *Chem. Phys. Lett.* **1980**, *70*, 343–349.
[79] P. C. Hariharan, J. A. Pople, *Theor. Chim. Acta.* **1973**, *28*, 213–222.
[80] P. C. Hariharan, J. A. Pople, *Mol. Phys.* **1974**, *27*, 209–214.
[81] W. J. Hehre, R. F. Stewart, J. A. Pople, *J. Chem. Phys.* **1969**, *51*, 2657–2664.
[82] W. J. Hehre, R. Ditchfield, J. A. Pople, *J. Chem. Phys.* **1972**, *56*, 2257–2261.
[83] G. A. Petersson, A. Bennett, T. G. Tensfeldt, M. A. Allaham, W. A. Shirley, J. Mantzaris, *J. Chem. Phys.* **1988**, *89*, 2193–2218.
[84] R. Cammi, B. Mennucci, J. Tomasi, *J. Phys. Chem. A* **2000**, *104*, 5631–5637.
[85] Gaussian 03, Revision C.02, M. J. Frisch, G. W. Trucks, H. B. Schlegel, G. E. Scuseria, M. A. Robb, J. R. Cheeseman, J. A. Montgomery, Jr., T. Vreven, K. N. Kudin, J. C. Burant, J. M. Millam, S. S. Iyengar, J. Tomasi, V. Barone, B. Mennucci, M. Cossi, G. Scalmani, N. Rega, G. A. Petersson, H. Nakatsuji, M. Hada, M. Ehara, K. Toyota, R. Fukuda, J. Hasegawa, M. Ishida, T. Nakajima, Y. Honda, O. Kitao, H. Nakai, M. Klene, X. Li, J. E. Knox, H. P. Hratchian, J. B. Cross, V. Bakken, C. Adamo, J. Jaramillo, R. Gomperts, R. E. Stratmann, O. Yazyev, A. J. Austin, R. Cammi, C. Pomelli, J. W. Ochterski, P. Y. Ayala, K. Morokuma, G. A. Voth, P. Salvador, J. J. Dannenberg, V. G. Zakrzewski, S. Dapprich, A. D. Daniels, M. C. Strain, O. Farkas, D. K. Malick, A. D. Rabuck, K. Raghavachari, J. B. Foresman, J. V. Ortiz, Q. Cui, A. G. Baboul, S. Clifford, J. Cioslowski, B. B. Stefanov, G. Liu, A. Liashenko, P. Piskorz, I. Komaromi, R. L. Martin, D. J. Fox, T. Keith, M. A. Al-Laham, C. Y. Peng, A. Nanayakkara, M. Challacombe, P. M. W. Gill, B. Johnson, W. Chen, M. W. Wong, C. Gonzalez, J. A. Pople, Gaussian, Inc., Wallingford CT, **2004**.
[86] Extensive work has been performed by Guldi and Martin[8,35,38–40,67] on dyads in which fullerene is a photoexcited electron acceptor and exTTF is the electron donor. For these systems, with an intrinsically larger driving force (0.7 eV, using the experimental two-electron value), the problem of the effective one-electron oxidation potential of exTTF is evidently much less critical than here.

Received: March 12, 2010
Published online: June 30, 2010

